REPRODUCIBLE DAYTIME SUPPRESSION AND NIGHT-TIME SURFACE ADVANTAGE IN A SOLAR-DRIVEN PCM RADIANT FLOOR: A CROSS-DAY PAIRED ANALYSIS.

Jurabek Kamolov[1], Sokhib Temirov[2,3], Marjona Makhmudova[3]

[1]PhD in Technical Sciences, Assistant Professor, Department of Engineering Technologies and Renewable Energy Sources, Bukhara State University, Bukhara 200117, Uzbekistan

[2]Assistant Professor, Department of Biomedical Engineering, Biophysics and Informatics, Bukhara State Medical Institute, Bukhara 200126, Uzbekistan

[3]Basic Doctoral Researcher, Department of Engineering Technologies and Renewable Energy Sources, Bukhara State University, Bukhara 200117, Uzbekistan

[3]Basic Doctoral Researcher, Bukhara State University, Bukhara 200117, Uzbekistan.

Abstract. Two parallel hydronic radiant-floor panels, a conventional concrete slab and a slab with eleven steel capsules filled with paraffin RT52, were driven by a parabolic solar concentrator and compared using paired temperature differences only. Over three independent test days, the PCM-integrated surface was cooler during charging by 1.32 ± 0.31 °C on average, and the return water by 0.69 ± 0.25 °C. In both long-duration tests the sign later reversed, with a maximum surface advantage of 1.25 and 1.07 °C about 3.8– 4.0 h after heat-flow reversal. The results show reproducible thermal-load shifting by the PCM-integrated assembly under real solar forcing.

Keywords: radiant floor; RT52; solar heating; thermal-load shifting; paired measurement; reproducibility.

Introduction. Low-temperature radiant floors are natural partners for solar heat, but solar supply is strongly time-varying, while the heating demand of a building peaks in the evening and at night. Phase change materials (PCMs)

embedded in the floor slab can, in principle, absorb part of the midday heat and release it later, thereby shifting the thermal response toward the period of demand [1–5]. Most published evidence, however, comes from laboratory chambers, electric heating mats or numerical models with a prescribed heat input [3–6], whereas outdoor solar experiments are exposed to fluctuating irradiance and changing inlet temperatures [7,8].

Under such non-stationary forcing, the absolute temperature of a single panel says little about the effect of the PCM. A more informative approach is to compare two panels that share the same supply water and the same weather at every instant. This thesis reports such a paired comparison and asks a narrow, experimentally answerable question: does the PCM-integrated floor reproducibly change the timing of its surface response, and if so, by how much and with what delay?

Experimental setup and metrics. A parabolic concentrator with a reflector area of 2.0 m^2 heated water in a copper spiral receiver. The water, with a total mass flow of 0.026 kg s^{-1}, was split between two panels of 1.20 × 0.60 m, each with 7.7 m of 16 × 2 mm PERT-AL-PERT pipe. The reference slab was 0.080 m thick; the PCM slab was 0.105 m thick and contained eleven RT52-filled steel tubes. The pump ran continuously, including at night. Supply (T_1), return (T_2, T_3) and surface (T_4, T_5) temperatures were logged on 3–4 July, 11 June and 13 June 2025, and a thermal camera provided an independent surface check.

The paired surface and return-water differences remove the shared supply temperature from the comparison:

$$\Delta T_s = T_5 - T_4, \qquad \Delta T_w = T_3 - T_2 \tag{1}$$

Because the logging interval was not uniform, charging-period means were time-weighted, and the persistence of the night-time advantage was quantified after the system-level reversal time t_{rev}:

$$\overline{\Delta T} = \frac{1}{t_b - t_a}\int_{t_a}^{t_b} \Delta T(t)\,\mathrm{d}t, \qquad I_{\mathrm{pos}} = \int_{t_{\mathrm{rev}}}^{t_{\mathrm{f}}} \max\left[\Delta T_{\mathrm{s}}, 0\right]\mathrm{d}t \tag{2}$$

To align the thermal histories of different days, a system-level reversal indicator was defined from the common inlet and the mean of the two branch returns; its zero crossing marks the instant when the net water-to-floor driving direction changes sign, which under continuous pumping is not a pump shutdown:

$$S(t) = T_1(t) - \frac{T_2(t) + T_3(t)}{2}, \qquad S(t_{\mathrm{rev}}) = 0 \tag{3}$$

Each experimental day, not each sample, was treated as one replicate, so the day-level statistics are

$$\mu_d = \frac{1}{N_d}\sum_{j=1}^{N_d} \overline{\Delta T}_j\,, \qquad s_d = \sqrt{\frac{1}{N_d - 1}\sum_{j=1}^{N_d}\left(\overline{\Delta T}_j - \mu_d\right)^2} \tag{4}$$

This choice avoids the artificially small p-values that would result from treating hundreds of autocorrelated samples as independent observations. For a difference of two independent channels with standard uncertainties u_i and u_j, and for the agreement between the infrared (ΔT_{IR}) and contact-sensor differences at N common timestamps, we use

$$u_{\Delta T} = \sqrt{u_i^2 + u_j^2}, \qquad C_{\mathrm{sign}} = \frac{1}{N}\sum_{k=1}^{N} \mathbf{1}\left[\mathrm{sgn}\left(\Delta T_{\mathrm{IR},k}\right) = \mathrm{sgn}\left(\Delta T_{\mathrm{s},k}\right)\right] \tag{5}$$

The documented sensor accuracy is approximately ± 0.2 to ± 0.5 °C depending on sensor type; it was used as a sensitivity bound rather than as a calibration certificate. Several physically impossible T_4 readings of 85 °C in the 11 June record were removed without replacement, and long logging gaps were not bridged by interpolation.

Results and discussion.

Daytime suppression is reproducible. On all three days the PCM-integrated surface and its return water were cooler than the reference during

charging (Fig. 1). The surface means were -1.220, -1.661 and -1.068 °C, giving $\mu_d = -1.32$ °C and $s_d = 0.31$ °C. The water-side means were -0.588, -0.515 and -0.971 °C ($\mu_d = -0.69$ °C, $s_d = 0.25$ °C). The between-day scatter is much smaller than the effect itself, and the sign never changed. The surface signal is roughly twice the water-side signal, which is expected: the return water is dominated by the common hydronic forcing, while the surface integrates the slower storage processes inside the slab.

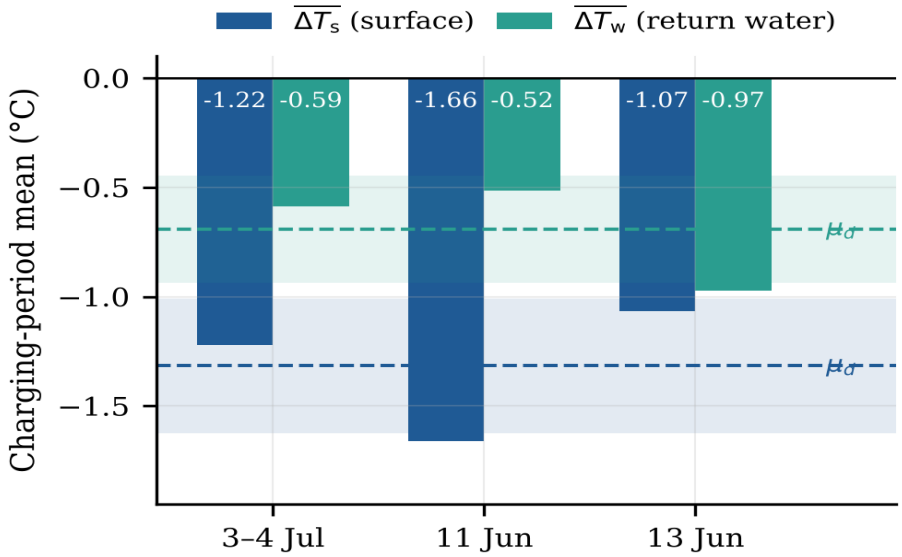

Fig. 1. Charging-period time-weighted paired differences on the three test days. Dashed lines show the day-level means μ_d; shaded bands show $\mu_d \pm s_d$.

The sign reverses after sunset. The full 3–4 July cycle is summarized as an event timeline in Fig. 2. The reference surface peaked at 46.13 °C at 16:56, and the PCM surface peaked 30 min later at 45.13 °C. The water-side driving direction reversed at about 17:15 while the pump kept running, so the floors began to return heat to the circulating water. The surface difference crossed zero at 18:47 and reached $+1.25$ °C at 21:13, i.e. $\tau_{max} = 3.96$ h after reversal. The PCM-integrated surface then remained warmer until the end of the record: the positive state lasted about 11.2 h, with $I_{pos} \approx 9.37$ °C · h. On 13 June the maximum advantage was $+1.07$ °C after 3.76 h, which is a close repetition despite a different thermal history. The peak delay of 30 min, in

contrast, was not repeated on 13 June and should be treated as a single-day observation.

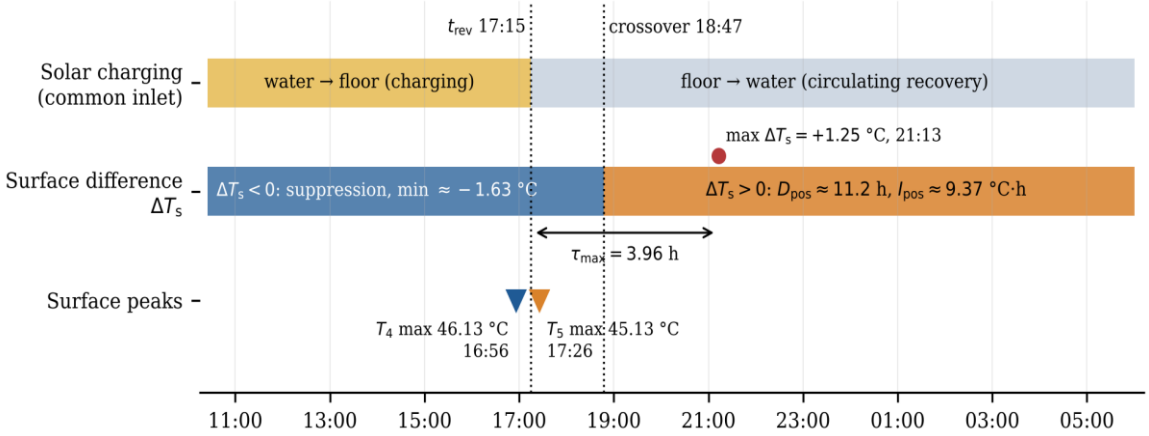

Fig. 2. Event timeline of the 3–4 July cycle: water-side regime, sign of the surface difference and surface-temperature peaks.

The main quantitative results are collected in Table 1. The two long-duration tests agree closely in the size and timing of the night-time advantage, whereas peak attenuation and peak delay are less repeatable and are therefore given only as descriptive values.

Table 1. Summary of paired-response metrics for the two long-duration tests.

Table-1

Metric	**3–4 July**	**13 June**
Charging-period $\overline{\Delta T_s}$, °C	−1.220	−1.068
Charging-period $\overline{\Delta T_w}$, °C	−0.588	−0.971
Maximum ΔT_s after reversal, °C	+1.25	+1.07
Lag τ_{max} after reversal, h	3.96	3.76
Positive-state duration D_{pos}, h	≈ 11.2	gap in record
Persistence integral I_{pos}, °C · h	≈ 9.37	gap in record

Independent confirmation. Infrared thermography, which has a different spatial footprint and different error sources from the contact sensors, showed the same daytime-negative to night-time-positive transition. After time alignment the two differential series correlated with $r = 0.87$ and agreed in

sign at 90% of the common timestamps ($C_{\text{sign}} = 0.90$). The infrared magnitudes are not a one-to-one substitute for the contact-sensor values, because the camera and the sensors do not see the same surface area; the camera is therefore used to confirm the sign and timing of the transition rather than its exact size.

Robustness to sensor error. Even if each sensor carried the largest documented bias of ± 0.5 °C in opposite directions, the worst-case error of a difference would be ± 1.0 °C. The three-day mean suppression (-1.32 °C) and the maximum night-time advantage ($+1.25$ °C) both exceed this bound, so their signs are not an artefact of sensor offsets, although their magnitudes carry a corresponding uncertainty. The fact that three days with different solar histories produce the same sign pattern is a further argument against a constant sensor offset as the explanation.

Interpretation. The combination of daytime suppression and a delayed positive surface response is the signature of thermal-load shifting: part of the surface heat release moves from the period of strong solar input into the evening and night, which is when a dwelling needs it [1,2,7]. The finding is reported as an effect of the whole PCM-integrated assembly. The PCM slab is also 2.5 cm thicker and contains steel tubes, so the measured differences combine extra sensible capacity, altered conduction paths and latent heat [9]. Separating these contributions requires a dedicated counterfactual analysis and is outside the scope of this paired measurement.

Practical relevance. For a solar-assisted floor, a 1– 1.3 °C lower surface temperature at midday reduces the risk of overheating and of excessive surface temperatures when the collector output is high, while a warmer surface in the evening covers part of the heating demand after the solar input has ended. The four-hour lag between heat-flow reversal and the maximum advantage is a useful design figure: it indicates the time scale on which this assembly redistributes heat, and it can be compared with the occupancy and demand

profile of a building when the PCM layer thickness, melting range and pipe spacing are chosen [2,5].

Limitations. Only three days were available, two of them long enough to observe the night-time phase, and the 13 June record contains a long overnight gap. Branch flow rates and room temperature were not logged as time series, which is why the analysis was confined to paired temperature observables.

Conclusions

Paired temperature differences measured on three independent days show that a solar-driven radiant floor with macroencapsulated RT52 reproducibly suppresses its surface temperature during charging (-1.32 ± 0.31 °C) and develops a positive night-time surface advantage of up to 1.25 °C about four hours after heat-flow reversal, lasting for about 11 h. The result is robust to the shared weather forcing and is confirmed by infrared thermography. Longer measurement campaigns with more test days and a geometry-matched reference slab are the next step toward quantifying the latent contribution itself.

REFERENCES.

[1] Rebelo F, Brett M, Figueiredo A, Vicente R, Simões N, Almeida RMSF, Ferreira VM. Experimental evaluation of a radiant floor system incorporating macroencapsulated phase change materials for improved heating and cooling performance. Energy. 2026;360:141692. https://doi.org/10.1016/j.energy.2026.141692.

[2] Rebelo F, Figueiredo A, Vicente R, Almeida RMSF, Ferreira VM. Experimental analysis of a radiant floor system incorporating phase change materials: Thermal performance and energy efficiency. Journal of Energy Storage. 2024;102:114084. https://doi.org/10.1016/j.est.2024.114084.

[3] Lin K, Zhang Y, Xu X, Di H, Yang R, Qin P. Experimental study of under-floor electric heating system with shape-stabilized PCM plates. Energy

and Buildings. 2005;37:215-220. https://doi.org/10.1016/j.enbuild.2004.06.017.

[4] Chen W, Liu Y, Liang X, Luo F, Liao T, Wang S, Gao X, Zhang Z, Fang Y. Experimental and numerical investigations on radiant floor heating system integrated with macro-encapsulated phase change material. Energy. 2023;282:128375. https://doi.org/10.1016/j.energy.2023.128375.

[5] Zhou D, Zhao CY, Tian Y. Review on thermal energy storage with phase change materials (PCMs) in building applications. Applied Energy. 2012;92:593-605. https://doi.org/10.1016/j.apenergy.2011.08.025.

[6] Li J, Xue P, He H, Ding W, Han J. Preparation and application effects of a novel form-stable phase change material as the thermal storage layer of an electric floor heating system. Energy and Buildings. 2009;41:871-880. https://doi.org/10.1016/j.enbuild.2009.03.009.

[7] Qiao X, Kong X, Fan M. Phase change material applied in solar heating for buildings: A review. Journal of Energy Storage. 2022;55:105826. https://doi.org/10.1016/j.est.2022.105826.

[8] Khamraev S, Kamolov B, Tadjiboyev S, Axmedova B, Burieva N, Ochilov M, Samatova S, Sharopov U. Experimental and theoretical analysis of thermo-hydraulic performance of a solar-collector-based hydronic floor heating system under climatic conditions of Uzbekistan. Energy. 2026;348:140399. https://doi.org/10.1016/j.energy.2026.140399.

[9] Rathore PKS, Shukla SK. Potential of macroencapsulated PCM for thermal energy storage in buildings: A comprehensive review. Construction and Building Materials. 2019;225:723-744. https://doi.org/10.1016/j.conbuildmat.2019.07.221.